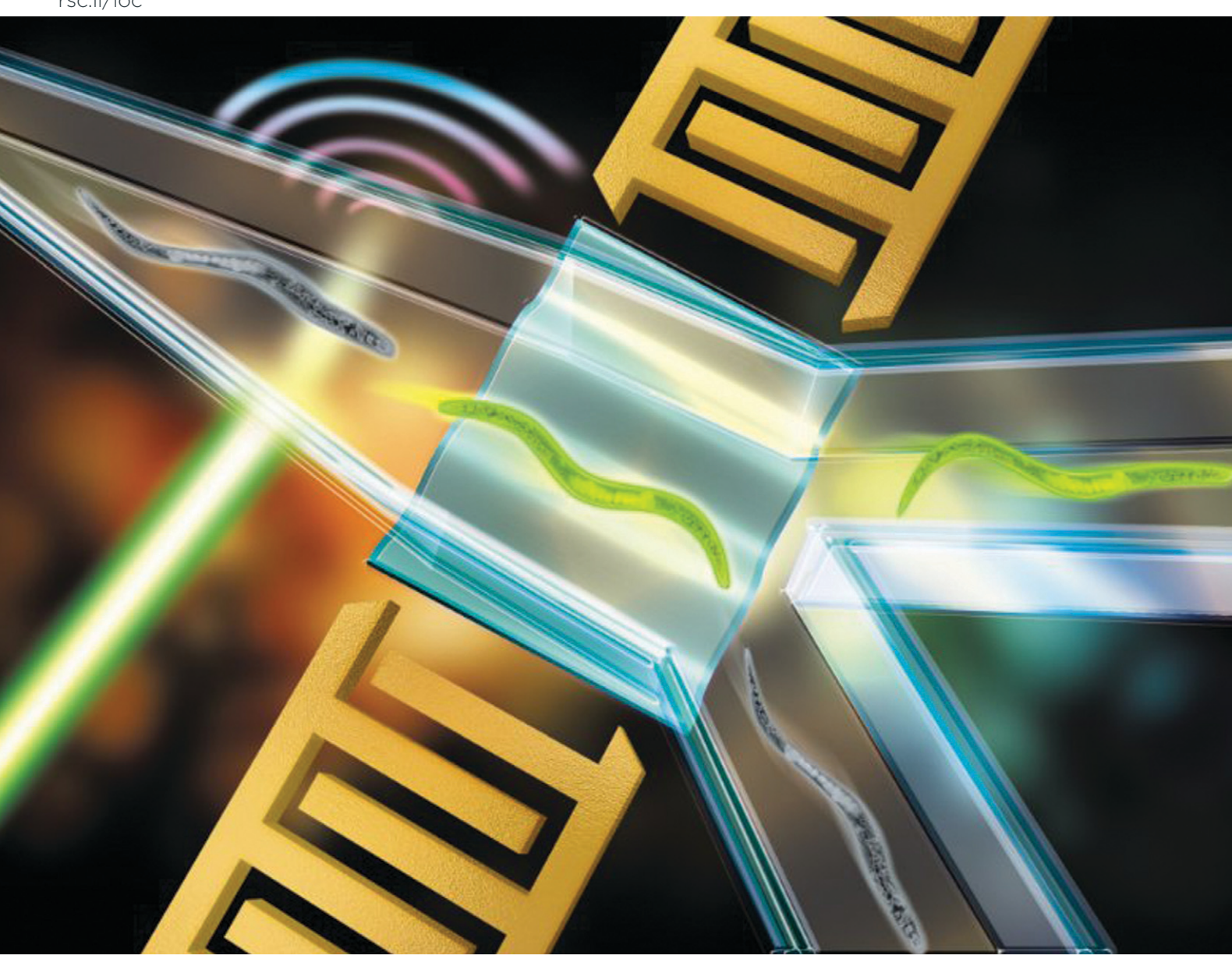
Volume 20 Number 10 21 May 2020 Pages 1697-1880

# Lab on a Chip

Devices and applications at the micro- and nanoscale rsc.li/loc



ISSN 1473-0197



#### PAPER

# Lab on a Chip



View Article Online **PAPER** 



Cite this: Lab Chip, 2020, 20, 1729

# Fluorescence-based sorting of Caenorhabditis elegans via acoustofluidics†

Jinxin Zhang, <sup>a</sup> Jessica H. Hartman, <sup>Db</sup> Chuyi Chen, <sup>a</sup> Shujie Yang, <sup>a</sup> Qi Li, <sup>a</sup> Zhenhua Tian, <sup>a</sup> Po-Hsun Huang, <sup>a</sup> Lin Wang, <sup>c</sup> Joel N. Meyer <sup>b</sup> and Tony Jun Huang <sup>1</sup> \*\* <sup>a</sup> \*\* <sup>b</sup> \*\* <sup>a</sup> \*\* <sup>a</sup> \*\* <sup>a</sup> \*\* <sup>b</sup> \*\* <sup>a</sup> \*

Effectively isolating and categorizing large quantities of Caenorhabditis elegans (C. elegans) based on different phenotypes is important for most worm research, especially genetics. Here we present an integrated acoustofluidic chip capable of identifying worms of interest based on expression of a fluorescent protein in a continuous flow and then separate them accordingly in a high-throughput manner. Utilizing planar fiber optics as the detection unit, our acoustofluidic device requires no temporary immobilization of worms for interrogation/detection, thereby improving the throughput. Implementing surface acoustic waves (SAW) as the sorting unit, our device provides a contact-free method to move worms of interest to the desired outlet, thus ensuring the biocompatibility for our chip. Our device can sort worms of different developmental stages (L3 and L4 stage worms) at high throughput and accuracy. For example, L3 worms can be processed at a throughput of around 70 worms per min with a sample purity over 99%, which remains over 90% when the throughput is increased to around 115 worms per min. In our acoustofluidic chip, the time period to complete the detection and sorting of one worm is only 50 ms, which outperforms nearly all existing microfluidics-based worm sorting devices and may be further reduced to achieve higher throughput.

Received 15th January 2020, Accepted 30th March 2020

DOI: 10.1039/d0lc00051e

rsc.li/loc

# Introduction

Caenorhabditis elegans (C. elegans) is highly valuable in studies of genetics, drug development, and cell biology due to its short (3 day) life cycle, overlapping homology with humans (~60%), small size, and ease of lab cultivation. 1-3 In particular, because of its well mapped anatomy, short generation time, and easy-to-operate genetics, C. elegans has significantly contributed to genetics, including gene pattern analysis, phenotyping, protein localization, and understanding gene expression.4-8 During analysis, large quantities of C. elegans are commonly used with each variation of assay, which becomes more efficient when green fluorescent protein (GFP) reporter gene constructs are added to C. elegans, because GFP can be an identifier when researchers select genotypes, verify genetic difference, and determine gene production localization. 8-10 For two decades, researchers have used GFP to mark notable

Except for the traditional method of manually picking C. elegans under a fluorescent dissecting microscope, which is both labor and time-intensive, 3,8 the first commercially available automated worm sorting platform, called "COPAS", and its subsequent advanced platform, called "BioSorter", have been developed by Union Biometrica.<sup>3,9</sup> These platforms are based on fluorescence-activated cell sorting (FACS) technology using a capillary system, which are not only challenging to operate and maintain, but also prohibitively expensive for labs and researchers.3,5 Alternatively, various microfluidic devices have been developed for the highthroughput C. elegans imaging, screening and sorting in the past years. 1,3,4,6,7,9,13-23 Chung et al. designed an integrated and automated C. elegans sorting microfluidic chip using multilayer PDMS valves in 2008.6 Although this chip could sort worms based on subcellular phenotypes with high accuracy, its throughput is low (~0.25 worms per second) and the mechanical immobilization process may induce stress in C. elegans, and thus cause damage to the worms, which is the common problem of the PDMS valves based

phenotypes that require more inquiry;8,10-12 therefore, the ability to isolate phenotypes based on GFP expression is incredibly useful. However, the needed ability to isolate and categorize large quantities of worms based on GFP difference is lacking by current mechanisms, as they are often slow, expensive, and invasive. 1,3,6

<sup>&</sup>lt;sup>a</sup> Department of Mechanical Engineering and Materials Science, Duke University, Durham, NC 27708, USA. E-mail: tony.huang@duke.edu; Tel: +1 919 684 5728 b Nicholas School of Environment, Duke University, Durham, NC 27708, USA

<sup>&</sup>lt;sup>c</sup> Ascent Bio-Nano Technologies, Inc., Research Triangle Park, NC 27709, USA

<sup>†</sup> Electronic supplementary information (ESI) available: L3 worms sorting at a throughput around (Video S1) 70 worms per min, (Video S2) 120 worms per min, (Video S3) 210 worms per min, Video S4: L4 worms sorting at a throughput around 220 worms per min. See DOI:10.1039/d0lc00051e

Lab on a Chip **Paper** 

worm sorting device. Meanwhile, the throughput of this chip still had the potential to be improved. Yan et al. developed a fluorescent worm sorting chip by integrating optical fiber detection and laminar flow switching, which could sort GFPexpressing worms from wild-type worms in a continuous flow. However, the throughput of this chip ( $\sim 0.2$  worms per second) was still low and the switching process was relatively complex (controlled by multiple pumps) for operation. As a result, it is essential to develop an integrated worm sorting chip that is high-throughput, affordable, and biocompatible.

Here, we describe an integrated acoustofluidic worm sorting chip that can sort C. elegans in continuous flow in a high-throughput, high-accuracy, and high-biocompatibility manner. Our acoustofluidic device works by isolating the GFP-expressing worms by detecting their fluorescence, which then triggers surface acoustic waves (SAW) that push the detected target worms into the sample outlet. Using SAW to provide contact-free forces to move worms improves the biocompatibility of the worm-sorting process.22-35 Our device is based on a continuous flow system. This approach eliminates potential contact-based stress acting on worms from the mechanical immobilization method, reduces the risk of injury for worms, and shortens the time period for the sorting process. With our chip, L3 worms can be processed at a throughput of around 70 worms per min with a sample purity over 99%, which remains over 90% when the throughput is increased to around 115 worms per min. We have also demonstrated that the sorting process is biocompatible, safe, and does not seem to have effect on worm viability and reproduction. With these attributes, our acoustofluidic chip can fulfil many unmet needs in biological/ biomedical and drug discovery studies involving C. elegans.

# Device design and concept

Fig. 1a illustrates the whole system design and the working process of our acoustofluidic worm sorting system, which

includes three major parts: optical detection part, electric determination and execution part, and the acoustofluidic worm sorting chip. The schematic of our acoustofluidic worm chip (Fig. 1b) consists  $\mathbf{of}$ single-laver polydimethylsiloxane (PDMS) microfluidic channel featuring two inlets, for loading the C. elegans samples and buffer, and two outlets, respectively, for unloading GFP-expressing and wild-type worms, and two fiber chambers for fluorescent signal detection. In addition, a pair of interdigital transducers (IDTs) deposited on a lithium niobate (LiNbO<sub>3</sub>) substrate can be used to generate SAWs. During the sorting process, the mixture of GFP-expressing and wild-type worms are first loaded in the microchannel from the worm loading inlet. After being straightened by the channel, each worm then enters into the detection window, where two optical fibers are aligned to distinguish the genotypes of the worm and then generate corresponding optical signal. If a worm is identified to be the GFP-type worm, the interdigital transducers (IDTs) will be activated to generate SAWs to push the GFP-type worm to the desired outlet (i.e., the GFPexpressing worm outlet). Otherwise, the worm will flow into the wild-type worm outlet.

# Experimental

#### Device fabrication

The acoustofluidic worm sorting chip comprised a PDMS channel with two fiber chambers and a LiNbO3 substrate patterned with one pair of IDTs. The PDMS microchannel was fabricated by soft lithography with the height of 130 μm. One fiber chamber was perpendicular to the microchannel, while the other fiber chamber was 45° to the microchannel. These two chambers were aimed at the same position in the microchannel. An SU-8 master mold was first prepared by standard photolithography. A PDMS microchannel was then fabricated from the SU-8 master mold. Once finished, the microchannel was punched at predesignated positions to

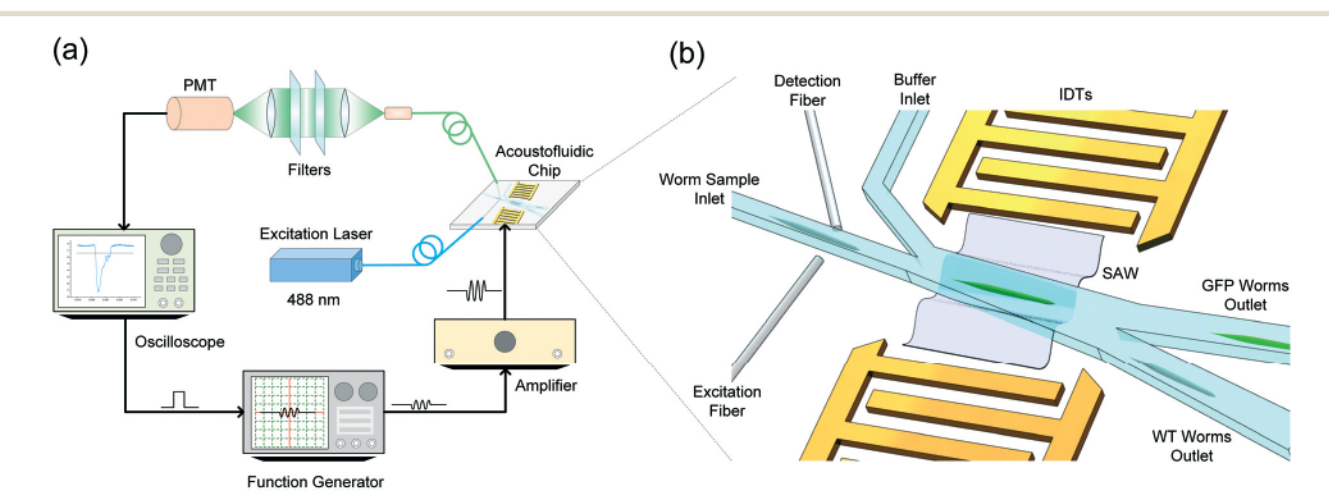


Fig. 1 Design and working process of the acoustofluidic C. elegans sorting system. (a) Schematic of the structure and working process of our acoustofluidic worm sorting system. (b) Schematic of our acoustofluidic worm sorting chip, which comprises a microchannel, a pair of optical fiber and a pair of IDTs.

open two inlets and two outlets for samples loading and unloading, respectively. To utilize the benefit of the tiltedangle standing SAW, 25 the worm loading straight channel with the width of 60 µm was tilted 12° to the SAWs' propagation direction. The IDTs were fabricated by standard photolithography, e-beam evaporation, and lift-off processes. To fabricate IDTs on LiNbO3 substrate, we first coated a LiNbO3 wafer (128° Y-cut, 500 µm thick) with a layer of SPR3012 photoresist (MicroChem, USA), followed by optical lithography and chemical developing. Then, chromium and gold layers (Cr/Au, 10/90 nm) were deposited on the LiNbO<sub>3</sub> substrate by e-beam evaporation, followed by the lift-off process to form one pair of IDTs. Both of the IDTs had 21 pairs of electrodes and their resonant frequency is 19.7 MHz with a wavelength of 200 µm. The spacing between each electrode was 50 µm and the aperture was 1.6 mm. The distance between two IDTs was 1.9 mm. Once both the PDMS channel and LiNbO3 substrate were prepared, they were treated with oxygen plasma and then bonded together, followed by incubation at 65 °C overnight.

#### Optical detection and signal control

The two optical fiber chambers are in-plane-integrated with the microchannel, with the width and height of 130 µm. Two multimode optical fibers (cladding diameter = 125 μm, core diameter = 105 µm, numerical aperture (NA) = 0.22, Thorlabs, USA) are first cleaved to get the flat ends and then inserted into these two chambers with an intersection angle of 135°; this angle was implemented to help reduce the influence of the excitation light. The excitation fiber is connected to a 488 nm laser (CrystaLaser, USA) to serve as the excitation source, while the detection fiber is connected to a photomultiplier tube (PMT, Hamamatsu C6780-20, Japan) for signal analysis. When a GFP-expressing worm comes through the detection part, it will be excited to generate the fluorescent light by the laser light coming from the excitation fiber. It is worth mentioning that the GFP-expressing worms can also be excited by the microscope fluorescent lamp, in which only the detection fiber is needed. The emitted fluorescent light can be collected by the detection fiber. Before transferred to the PMT, all the detected light should go through a bandpass filter (530/40 nm) to avoid the influence of the excitation light and environmental light (Fig. 1a).

The PMT is connected to a homemade Labview program, and the intensity of the detected fluorescent light can be converted to the corresponding voltage signal. The oscilloscope is used to display the signal and control the trigger signal. When a GFP-expressing worm passes by, a voltage peak will be displayed in the oscilloscope. After detecting the voltage peak by setting the threshold value, the oscilloscope can generate a trigger signal to turn on a function generator (AFG3011C, Tektronix, USA). After a short delay (according to the time required for a worm to move from the detection part to the sorting part), the radio frequency (RF) signal with a duration of around 50 ms is

amplified through an amplifier (25A250A, Amplifier Research, USA) and then applied to the IDTs to generate SAWs (Fig. 1a).

#### **Device operation**

The acoustofluidic worm sorting chip was mounted on an inverted microscope (TE2000-U, Nikon, Japan). The mixture of GFP-expressing and wild-type *C. elegans* was injected into the microchannel through 1 mL syringes (BD Bioscience, USA) administered by an automated syringe pump (neMESYS, Germany). K-medium buffer was also delivered by this pump through 5 mL syringes (BD Bioscience, USA). Images and videos were captured by a fast camera (Fastcam SA4, Photron, USA) through Photron FASTCAM Viewer (PFV, Photron, USA). All acquired images and videos were analyzed by ImageJ (NIH, USA).

## Preparation of C. elegans and result verification

Nematode growth medium agar (K-agar)<sup>36</sup> was prepared by first dissolving 2.36 g of KCl, 3 g of NaCl, 2.5 g of peptone, and 20 g agar in 1 L of distilled water, followed by autoclaving the mixture. Once the autoclaved mixture was cooled down to 55 °C, it was mixed with 1 mL 1 M CaCl<sub>2</sub>, 1 mL 1 M MgSO<sub>4</sub>, 1 mL 10 mg mL<sup>-1</sup> cholesterol, and 5 mL 1.25 mg mL<sup>-1</sup> nystatin to obtain the final K-agar. The K-agar was then poured on a petri dish and seeded with bacteria within 24 hours. K-medium buffer for *C. elegans* was made by adding 2.36 g of KCl and 3 g of NaCl into 1 L of distilled water and autoclaving the mixture.

The C. elegans life cycle begins at the embryonic stage and progresses through four larval stages (L1-L4) and adulthood. Eggs are typically laid 10-12 hours before they hatch, and they reach the L1, L2, L3, and L4 stages 14, 22.5, 31.5, and 42 hours after hatching, respectively.37 During this time, the animals undergo tremendous growth, such that an L4-stage worm is ~50% larger than an L3-stage worm.38 The size of the L3 worms is around 500-550 µm in length and 30-35 µm in diameter, and the size of L4 worms is around 700-800 µm in length and 45-50 µm in diameter. 39 In this study, we used L4 stage animals as this is one of the most common stages used in C. elegans research, both for its biological importance and for practical reasons since L3- and L4-stage animals are easily recognized under a dissecting microscope. We also used L3- and L4- stage animals to test the effect of size on the sorting effectiveness.

Both wild-type and transgenic *C. elegans* were tested in our devices. The N2 Bristol wild-type strain and SJ4103 [zcIs14; myo-3p:mtGFP] strains were obtained from the Caenorhabditis Genetics Center. Nematodes were maintained on K-agar plates at 20 °C. Synchronized populations of L3 and L4 larval stage nematodes were obtained by isolating embryos with bleach/sodium hydroxide treatment from the gravid adults on a 'full' plate of worms and overnight hatch for 16 h in food-free complete K-medium (with added MgSO<sub>4</sub>, CaCl<sub>2</sub>, and cholesterol). The amounts of eggs isolated to the

plate were assumed nearly uniform each time. Since the GFP worms have a slower rate of development and smaller brood size, 40 there is likely fewer gravid adults to begin with, so we had fewer eggs and worms in the GFP group. Afterward, synchronized L1 larvae were plated to K-agar plates with food for 36 h (L3 stage) or 48 h (L4 stage). On the day of the experiment, one plate of WT worms and one plate of GFP worms were washed from the plates separately in 13 mL K-medium and pelleted by centrifugation at 2200 rcf for 1 min. The supernatant was removed and replaced with 5 mL clean K-medium. Then, the two 5 ml worm solutions were mixed to obtain the 10 ml unsorted worm solution. The concentration of this worm solution can be estimated by imaging a small sample, as shown in Fig. S5;† the ratio of the GFP worms to WT worms was generally around 0.43: 0.57, and the worm concentration was around 800-1000 worms per ml. Before being loaded into the channel, nematodes were all paralyzed with sodium azide at a final concentration of 10 mM.

After sorting, the accuracy of sorting was determined by fluorescence microscopy. Briefly, >100 sorted animals were placed on a slide, covered with a cover slip, and the slide was imaged using a Keyence BZ-X700 all-in-one fluorescent microscope using brightfield and fluorescence detection with an EGFP filter. An overlay image of the fluorescence and brightfield was created using the BZ-X software and the number of GFP-expressing animals were manually counted in the images.

The effect of the sorting on the health of the worm was determined using two methods: lethality and reproduction. First, the sorted animals were rinsed three times with K-medium to remove the sodium azide paralytic, and they were placed on K-agar plates with food for 30 minutes. After 30 minutes recovery, lethality was determined by a harsh touch with a platinum wire. Animals were considered to be dead if they did not respond to three touches with the wire. Secondly, the larval animals were picked to reproduction plates (3 adults per plate, 3 plates per condition in each biological replicate) and allowed to lay eggs. The adults were transferred every day to new plates during reproduction and the larvae were counted after 48 h. Brood size was determined by summing all larvae from all days of reproduction and dividing by the number of adults.

Sorting accuracy, lethality, and reproduction were performed in three individual biological replicates.

# Results and discussion

## Worm type detection

After being injected into the microchannel, the worms first go through a gradually narrowed channel and then pass by the optical detection window. The 60  $\mu$ m wide channel is not only wide enough for the smooth passage for L3 and L4 worms, but also ensures that only one worm could flow through at a time. In addition, the smaller distance between worms and fibers can increase the detection accuracy. Fig. 2a shows the schematic of our optical detection mechanism; as

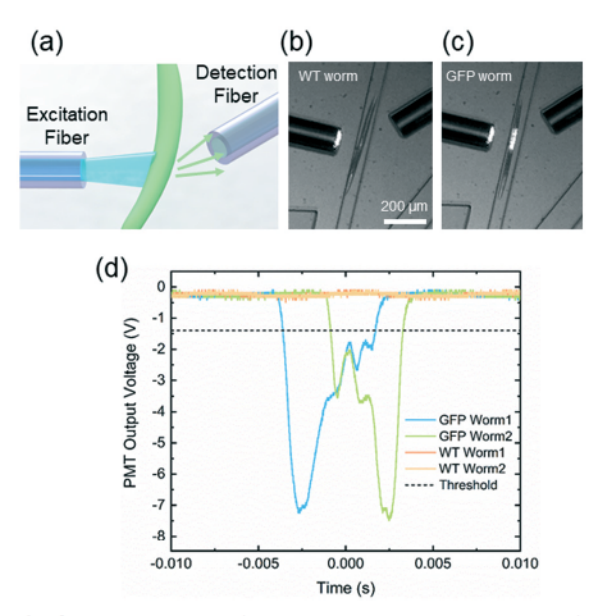


Fig. 2 Characterization of the optical detection part of our acoustofluidic worm sorting chip. (a) Schematic of the in-plane optical detection system when a worm passes by. (b) Optical image of the detection system when a wild-type L3 worm passes by. The left fiber is the excitation fiber, while the right fiber is the detection fiber. (c) Optical image of the detection system when a GFP-type L3 worm passes by. (d) Output voltages of the PMT when different worms pass by the optical detection part. GFP-type worms can cause the corresponding voltage peaks, while wild-type worms cannot.

mentioned before, when a GFP-expressing worm passes by the optical fiber region, the excited fluorescent light can be collected by the detection fiber and then transferred to the PMT. As shown in Fig. 2b and c, a wild-type L3 worm and a GFP-expressing L3 worm were passing through the optical detection region respectively.

Here, we used a homemade LabVIEW program to process the PMT signal and transfer this signal to the corresponding output voltage, which was displayed in the oscilloscope in real time. Fig. 2d displays the corresponding output voltage waveforms when different worms passed by the optical detection area. The GFP-expressing worms could cause obvious voltage peaks, while wild-type worms did not trigger recognizable waveform changes. Although the worm might pass by the optical detection area in a head-first manner (i.e., worm's head enters the area first) or a tail-first manner (i.e., worm's tail enters the area first), both corresponding output voltage waveforms could be used to trigger the function generator in the same method (Fig. 2d). This method is the falling edge trigger, i.e., the trigger signal is sent when the waveform crosses the threshold in a falling way. Furthermore, the choice of the threshold value should ensure that all the GFP-expressing worms can be detected and each GFPexpressing worm only generates one trigger signal. Threshold choice is critical; it would be possible to miss some GFPexpressing worms with weak fluorescence if a threshold with a high value were chosen. Furthermore, according to Fig. 2d, one GFP-expressing worm might generate more than one

Lab on a Chip **Paper** 

trigger signals if a threshold with a middle value was chose. Therefore, for the GFP-expressing strain we used in this experiment, a low value (-1.4 V) was chosen as the trigger threshold, as shown in Fig. 2d. It is worth mentioning that the threshold value should be chosen according to the specific strain used in the experiment, which means our acoustofluidic worm sorting chip has the potential for sorting fluorescent worms with different genotypes.

#### Acoustic worm sorting mechanism

After passing by the optical detection window, the worm arrives at the acoustic sorting area. As mentioned above, a GFP-expressing worm can trigger a temporary acoustic field, which can push this worm to the GFP-expressing worms' outlet (the upper outlet in Fig. 1b). Alternately, a wild-type worm will follow the original laminar flow to the wild-type worms' outlet (the lower outlet). To ensure that different worms arrive at their correct outlets, a buffer flow with a suitable flow rate is necessary. Here, we first numerically calculated the influence of different flow rate ratios (i.e., the ratio of worm flow rate to the buffer flow rate) through a COMSOL (Multiphysics 5.3, COMSOL Inc.) simulation. The worm flow was colored in red and the buffer flow was colored in blue. Fig. S1 in the ESI† shows the concentration

distribution result of the worm flow in the whole worm sorting area with a flow rate ratio of 1:2.5, which was used in our worm sorting experiment. This result indicated that, under this flow rate ratio, worms could be kept in the worm flow and then move through the wild-type worms' outlet if there was no other effect, as shown in Fig. 3a. Meanwhile, if the worm was pushed to the blue region, then the worm could come to the GFP-expressing worms' outlet. Other flow rate ratios' results and worm flow concentration distribution of the cross-section of the bifurcation part can be found in Fig. S1.† Higher buffer flow rate can help ensure the worm exit from the right outlet, however, excessively increasing the buffer flow rate might push worms to the channel wall and cause damage to the worms and a waste of buffer.

In order to study the acoustic pressure distribution induced by the SAW field in the sorting area, another numerical simulation was conducted based on our pervious reported model.41,42 Boundary condition settings and material properties were modified according to our device design. As shown in Fig. S2,† four pressure nodes are formed in the sorting area. Here, the acoustic radiation force is decided by the equation below:

$$F_{\rm r} = -\left(\frac{\pi p^2 V_{\rm p} \beta_{\rm f}}{2\lambda}\right) \varphi(\beta, \rho) \sin(2kL)$$

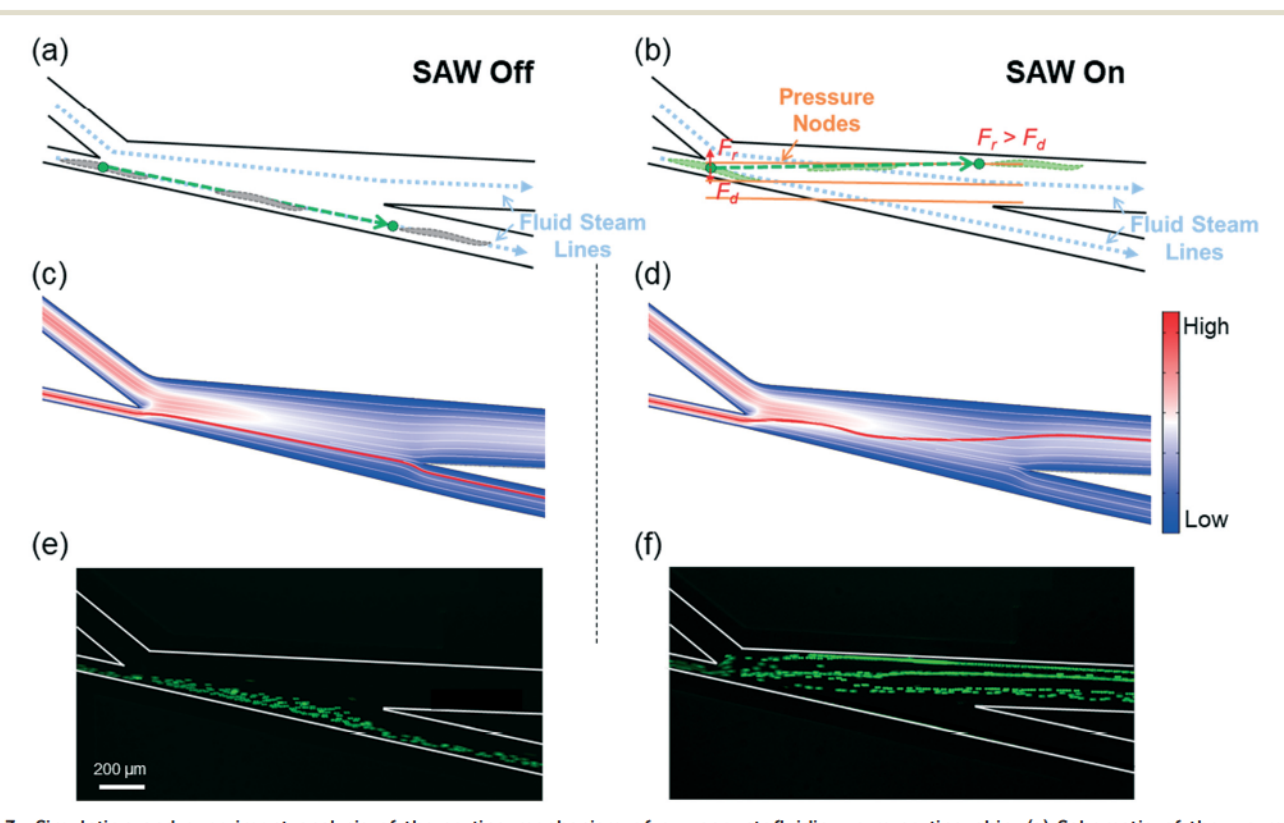


Fig. 3 Simulation and experiment analysis of the sorting mechanism of our acoustofluidic worm sorting chip. (a) Schematic of the worm and particle movement when acoustic power is off. (b) Schematic of the worm and particle movement when acoustic power is on, which illustrates our sorting mechanism with respect to relative forces. Simulation results of particle tracking (red line) when acoustic power is (c) off and (d) on. The background is the flow rate distribution; blue color represents low flow rate, while red means high. The white lines are the fluid stream lines. Experimental results of 10 µm fluorescent particle motions in the sorting area when acoustic power was (e) off and (f) on. The particles were introduced from the worm loading inlet with a flow rate of 20  $\mu$ l min<sup>-1</sup>, and the flow rate of buffer was 50  $\mu$ l min<sup>-1</sup>.

where p,  $V_p$ ,  $\lambda$ , k, and L are the pressure amplitude, particle volume, acoustic wavelength, wave vector, and distance from the pressure node, respectively.  $\beta$  is compressibility, and  $\rho$  is

density.  $\varphi$  is the acoustic contrast factor, which determines the direction of the acoustic radiation force.

$$\varphi(\beta, \rho) = \frac{5\rho_{\mathbf{p}} - 2\rho_{\mathbf{f}}}{2\rho_{\mathbf{p}} + \rho_{\mathbf{f}}} - \frac{\beta_{\mathbf{p}}}{\beta_{\mathbf{f}}}$$

where the subscripts p and f represent particle and fluid, respectively. Most particles and cells, such as polystyrene beads and blood cells, are experiencing the acoustic radiation force that pushed them towards the pressure nodes in the acoustic field because of their positive acoustic contrast factor  $\varphi$ . 27,43-45 According our previous work, 22 C. elegans also shows a positive acoustic contrast factor.

The mechanism of our acoustofluidic worm sorting method is displayed in Fig. 3b. When a worm comes into the standing acoustic field in the sorting area, the acoustic radiation force applied to the worm can push the worm the nearby pressure node. In the meantime, the drag force from the fluid tends to keep the worm motion aligned with the original fluid stream line. Therefore, the movement path of the worm can be determined by the balance of these two forces and finally aligned to the pressure node if acoustic radiation force is stronger, or follow the original fluid stream line if the acoustic power is off or the acoustic radiation force is negligible relative to the drag force. As shown in Fig. 3c and d, the simulation calculated the particle tracking results (red lines) when acoustic power was off and on, respectively. The backgrounds were flow rate distribution with fluid stream lines (white lines). When acoustic power was off, particles would follow the fluid stream line and come to the lower outlet. Conversely, particles would come to the upper outlet under the interaction with acoustic field when acoustic power is on.

To experimentally verify these simulation results and sorting mechanism, we introduced 10 µm diluted polystyrene microparticles with green fluorescence into the sorting channel from the worm loading inlet with a flow rate of 20  $\mu$ l min<sup>-1</sup>. The buffer flow rate was 50 μl min<sup>-1</sup> (2.5 times). When the acoustic power was off, all the particles followed the fluid stream lines and exited the sorting area from the wild-type worms' outlet, as shown in Fig. 3e. When an RF signal (19.7 MHz, 25.6 V<sub>pp</sub>) was applied to the ITDs to build the standing acoustic field in the sorting area, all the particles were aligned to the three pressure nodes and then exited the sorting area from the upper outlet, as shown in Fig. 3f. These experimental results were well-matched with the simulation results.

#### High-throughput acoustic C. elegans sorting

In order to demonstrate the sorting performance of our acoustofluidic worm sorting chip, worms at two different developmental stages (L3 and L4 larval worms) were sorted separately at different throughputs. We first sorted a mixture of L3 wild-type worms and GFP-expressing worms at a throughput of around 70 worms per min. The flow rate in the worm loading channel was around 20 µl min-1, and the flow rate of the buffer was set to be 2.5 times faster. The power to generate acoustic field was 25.6 Vpp. Fig. 4 displays the sorting processes of a wild-type worm and a GFP-expressing worm under this configuration. When a wild-type worm passed by the optical detection part, the PMT output was not changed obviously, and thus no trigger signal was sent to the function generator. Therefore, no acoustic field was built, and the worm exited the sorting part via the wild-type worm outlet (Fig. 4a and b). However, when a GFP-expressing worm was detected at the optical fiber area, as we introduced above, the PMT output crossed the threshold and a trigger signal was then sent to the function generator to generate a RF signal with suitable delay time and duration. After amplification, this signal was sent to the IDTs to apply the acoustic field to push the worm to the GFP-expressing worm outlet (Fig. 4c and d). To enhance the sorting accuracy, the acoustic field should be built completely as the GFP-expressing worm begins to enter the sorting area. Here, the delay time was set to 5 ms because it took at least 5 ms for the worm to move from the optical detection area to the entrance of the acoustic sorting area (Fig. 4c and d). The acoustic field can be seen as the black and white stripes in Fig. 4c, in which the white stripes indicated the pressure nodes. Corresponding to the simulation and particle experiment results, the GFPexpressing worm was pushed to the pressure node after it entered the acoustic field and followed the pressure node as it exited the sorting area (Fig. 4c). Higher throughputs for L3 worms have been tested by our chip using higher flow rates, as shown in Videos S1-S3.† For both types of L3 worms, the whole detection and sorting process took around 50 ms, which corresponds to a theoretical maximum soring rate of more than 1000 worms per min.

In addition to the L3 worm sorting, we also sorted L4 worms using the same device. Because L4 worms are longer and heavier than the L3 worms, the acoustic power was increased (31.2 Vpp) to improve the acoustic radiation force, and thus increase the sorting accuracy. Other experimental conditions remained the same. Similar to the L3 worms, an L4 wild-type worm could directly pass by the detection part and follow the original fluid stream line exit via the wild-type worm outlet, as shown in Fig. S3a and Video S4.† It is worth noting that some wild-type worms may display a flash of light when they pass through the optical detection area because the video is captured by the fast camera; however, this flash light cannot pass the filters. Furthermore, a GFP-expressing L4 worm could be detected at the optical detection area and then be pushed to the pressure node in the standing acoustic field, and finally exit via the GFP-expressing worms' outlet, as shown in Fig. S3b and Video S4.† The whole detection and sorting process of L4 worms took around 60 ms. Although this time was a little longer than L3 worms, corresponding theoretical maximum sorting rate can also reach 1000 worms per min.

**Paper** 

Lab on a Chip

(a) WT Worm (C) GFP Worm 5 ms 20 ms 0 ms 5 ms 20 ms 50 ms 0 ms 50 ms (d) (b) 8 (V) 8 Voltage (V) Voltage (V)

Fig. 4 Acoustic sorting process of L3 worms. (a) Image sequence displaying the detection and sorting process of an L3 wild-type worm. (b) The corresponding signal changes when the wild-type worm shown in (a) pass by the chip. When a wild-type worm passed by the detection part, the PMT output did not change obviously and thus no trigger signal was sent to the function generator, therefore, no RF signal was applied to the IDTs. (c) Image sequence of a GFP-expressing L3 worm detected and then sorted by acoustic field. (d) The corresponding signal changes when the GFP-expressing worm shown in (c) pass by the chip. When a GFP-expressing worm passed by the detection part, the PMT output could cross the detection threshold and thus a trigger signal was sent to the function generator immediately; therefore, an RF signal with a certain duration (50 ms) was then applied to the IDTs after a designed delay (5 ms). Yellow triangles point out the position of the worms. Gray arrows link the optical images and their corresponding time points.

PMT Output

- Threshold

0.045

0.040

#### Characterization of the C. elegans sorting results

0.000

To characterize the performance of our acoustofluidic worm sorting chip, GFP-expressing worms were set as the target sorted from wild-type worms at different throughputs. After the worms were sorted using our acoustofluidic method, we then calculated and analyzed the sorting purity and yield based on the equation listed below:

$$Purity = \frac{\text{Number of sorted GFP worms}}{\text{Number of total sorted worms}}$$

$$Yield = \frac{Number of sorted GFP worms}{Number of detected sorted worms}$$

Because the concentration of the worm solution used in the every experiment was approximate, the throughput was modified by changing the worm loading flow rate. At the lowest flow rate we used, sorting purities and yields of L3 and L4 worms of nearly 100% were achieved when the throughput was around 70 worms per min. Fig. 5a-d shows representative results from a single experiment under these configurations. The sorted worms were collected from different outlets and then imaged with a fluorescent microscope to obtain the overlaid fluorescence and bright field microscope images, which were then used for calculation of purity and yield. Nearly all worms from GFPexpressing worm outlets showed green fluorescence while

most worms from wild-type worm outlets did not show green fluorescence, in both L3 and L4 staged animals. Fig. 5e and f displayed the purity and yield of L3 and L4 worms at different throughputs separately (compiled data from 3 replicates). For L3 worms, though the purity and yield decreased with the increase of throughput, they still remained higher than 90% at the throughput of around 115 worms per min, and higher than 80% at the throughput of around 155 worms per min. At higher flow rates, the purity and yield dramatically decreased with the increase of throughput, reaching roughly 60% at the throughput of around 210 worms per min. For L4 worms, although their purity and yield were slightly lower than L3 worms, their data displayed the same tendency.

PMT Output

0.050

Threshold

0.045

0.040

Here, the main reason for the decrease in purity is most likely the increased chance that multiple worms pass by the sorting area together or one-after-another. Though the distance between neighboring worms is kept constant in the detection channel, the worms slow down suddenly when they enter the sorting channel due to the substantial increase in the channel width. The change of the flow rate distribution in the channel can be seen in the simulation results in Fig. 3c and d. The average time that worms spent in the sorting unit decreased from around 55 ms to around 35 ms for L4 worms when the flow rate for the worm solution increased from 20 µl min-1 (low-throughput condition) to 60 μl min<sup>-1</sup> (high-throughput condition), which indicated that the increase in worm speed in the sorting channel was less

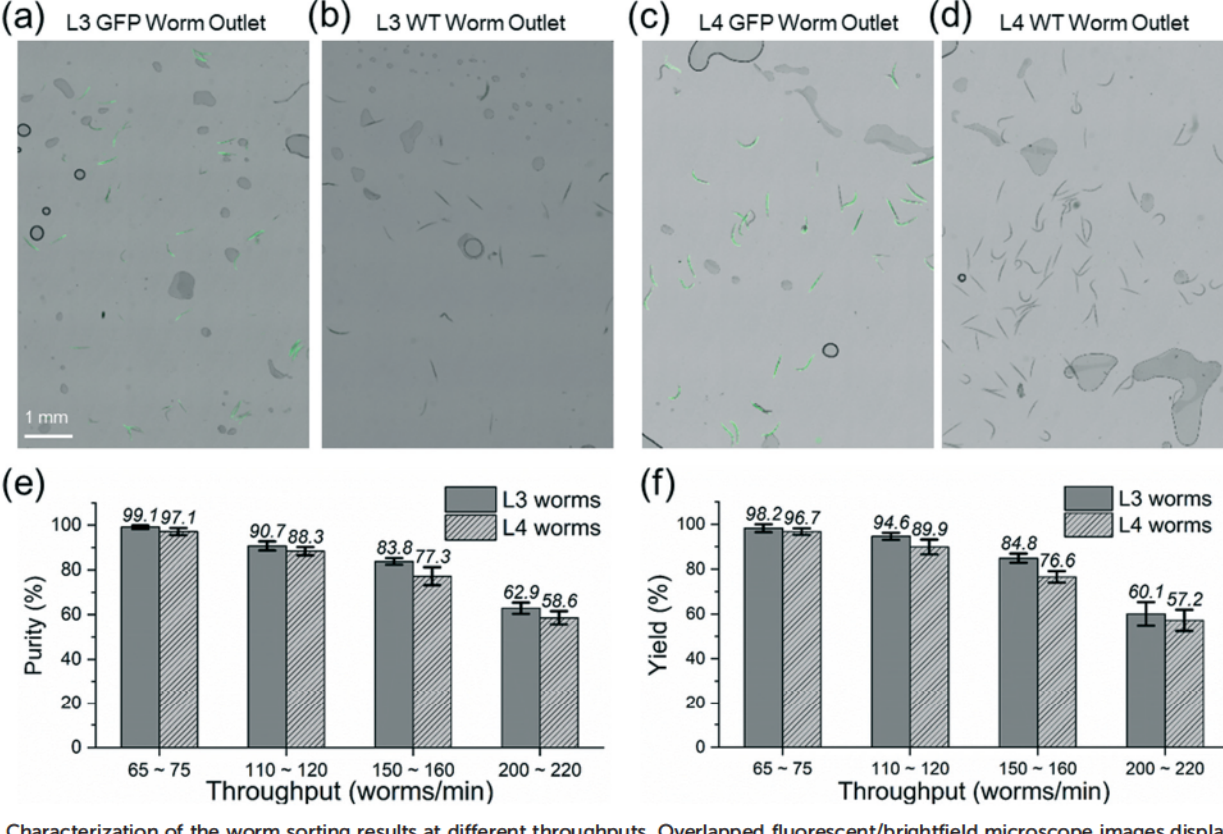


Fig. 5 Characterization of the worm sorting results at different throughputs. Overlapped fluorescent/brightfield microscope images displaying the L3 worms collected from the (a) GFP-type worm outlet and (b) wild-type worm outlet in a L3 worm sorting experiment at a throughput of around 70 worms per min. Overlapped microscope images displaying the L4 worms collected from the (c) GFP-type worm outlet and (d) wild-type worm outlet in a L4 worm sorting experiment at a throughput of around 70 worms per min. To better display the results, the pictures shown here were cropped; complete pictures can be found in Fig. S4.† (e) The purity of the L3 and L4 worms sorted at different throughputs. (f) The yield of L3 and L4 worms sorted at different throughputs.

than that in the detection channel. Under these circumstances, the worms entering the sorting channel with a higher initial velocity will have a shorter distance between neighboring worms. Therefore, there was an increasing chance that multiple worms passed by the sorting area closer together with an increase in the flow rate; worms that pass the deflection region near a GFP-expressing worm may be pushed to the GFP-expressing worm outlet in error, negatively impacting the purity. Since the minimum width for deflecting a GFP-expressing worm was constrained by the diffraction limit of the acoustic wave, a minimum distance between neighboring worms was required to maintain a high purity.

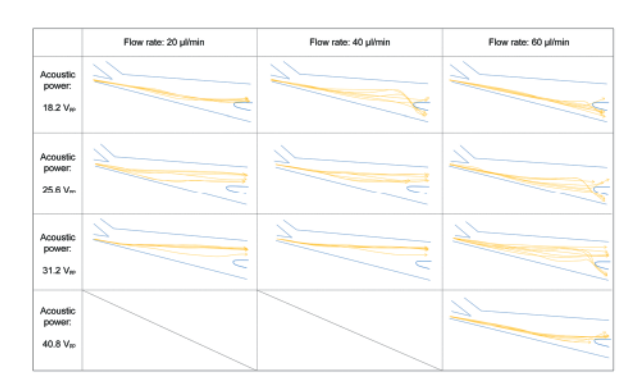
Furthermore, the flow rate increase not only reduced the purity, but also decreased the yield, which was mainly due to the rapid increase of the drag force applied on the worms and the diminishing time that the worms spent in the sorting area (acoustic field). The drag force applied to the worm from the fluid can be expressed as:

$$F_{\rm d} = -3\pi \eta dv$$

where  $\eta$  is the viscosity of the fluid, d is the diameter of the particle, and  $\nu$  is the relative velocity of particle with respect to

the fluid. The increase of the flow rate will only increase the drag force, but not the acoustic radiation force applied to the worms. Therefore, when the worm was deflected by the acoustic radiation force to deviate from the original fluid stream line, the drag force applied to the worm abruptly increased due to the increase of relative velocity, which reduced the success rate and thus reduced the yield. Besides, the increase of flow rate also reduced the time the worm was exposed to the acoustic field, resulting in the decrease of yield.

To demonstrate the relationship between drag force and acoustic radiation force applied to the worms, wild-type L4 worms were flowed into the sorting channel with different flow rates ranging from 20  $\mu$ l min<sup>-1</sup> to 60  $\mu$ l min<sup>-1</sup> while different acoustic powers were applied to the worms. Then, the trajectories of the worms under different flow rate and acoustic power conditions were tracked and recorded, as shown in Fig. S7–S10† and summarized in Fig. 6. When acoustic power was relatively low (18.2 V<sub>pp</sub>), L4 worms could only be completely pushed to the right outlet when flow rate was low (20  $\mu$ l min<sup>-1</sup>). With an increase in the flow rate, the effect of the acoustic radiation force applied on the worms became much lower compared to the drag force (Fig. S7†), which could explain why the yield quickly decreased when



Lab on a Chip

Fig. 6 Summary of all the trajectories (experimental results) of the L4 worms passing through the sorting area in different flow rates when different acoustic powers were applied. The blue lines are the contours of the sorting area of the microchannel, and each yellow line represents a trajectory of a worm. Detailed image stacks can be found in Fig. S7–S10.†

flow rate increased. When the acoustic power was increased to a moderate level (25.6 Vpp), which was used for L3 worm sorting in our experiments, different from the low power circumstance, all the L4 worms in the moderate flow rate (40 μl min<sup>-1</sup>) and around half of the L4 worms in the high flow rate (60 µl min<sup>-1</sup>) could be pushed to the desired outlet (Fig. S8†). Furthermore, more than half of the L4 worms in the high flow rate (60 µl min<sup>-1</sup>) could be pushed to the right outlet when acoustic power was increased to 31.2  $V_{\rm pp}$  (Fig. S9†), which was used for L4 worms sorting in our experiments. Therefore, increasing acoustic radiation force applied to the worms by increasing the acoustic power could improve the yield when the flow rate is high; additionally, all of these acoustic powers were confirmed as safe for the worms. Although higher acoustic power can achieve a higher yield, as nearly all the L4 worms could be pushed to the desired outlet in high flow rate (60 µl min<sup>-1</sup>) when we increasing the acoustic power to 40.8  $V_{pp}$  (Fig. S10†), worms were occasionally observed damaged due to the shock heat from the high acoustic power. In summary, because the increase of the flow rate will only increase the drag force, but not the acoustic radiation force applied to the worms, we can correspondingly increase the acoustic power to improve the yield for high throughput worm sorting. However, further performance improvement would require modification to the channel, IDT, or experimental design when using excessively high acoustic power.

In addition to the acoustic power and flow rate, many other factors can influence the sorting performance, such as the concentration of worm solution, and different channel or IDT designs. Although a higher concentration can improve the yield and achieve a high throughput while avoiding using high flow rates, the purity may be impacted by the reduced spacing between neighboring worms. Here, we intend to demonstrate that our acoustofluidic worm sorting chips have the potential to satisfy different worm sorting requirements over a wide throughput range, where different chip designs and experimental parameters can be used for special applications to achieve optimized performance.

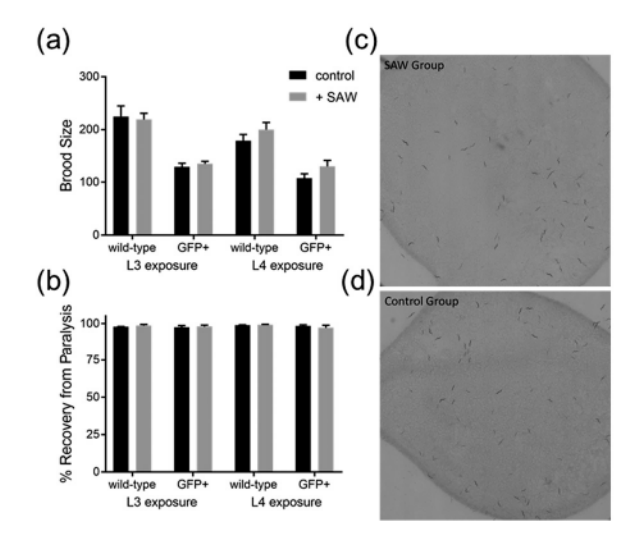


Fig. 7 Characterization of biological impact of sorting on worm physiology. To demonstrate physiological impact, total brood size (a) (number of offspring per individual worm) was measured for worms exposed to SAW during the L3 or L4 larval stages. Lethality (b) was also measured as total number of surviving animals after paralysis with sodium azide and exposure to SAW for sorting. Representative images for offspring from a single worm after 72 h of reproduction in worms exposed to SAW (c) or control (d). All experiments were performed in triplicate biological replicates with multiple technical replicates as described in Experimental methods.

## Biocompatibility of our acoustofluidic worm sorting chip

Following the sorting, the effects on the overall worm physiology were determined by the reproduction and lethality experiments (Fig. 7a-d). In reproduction experiments, there was no effect of acoustic wave sorting on total brood size compared to controls in either L3 or L4 stage groups, although GFP-expressing animals had a smaller brood size in general compared to the wild-type (Fig. 7a), which has been reported by the strain's original authors.40 The lethality of worms was determined as the percent of surviving worms after 30 minutes of recovery from sodium azide. There was >98% survival in all groups regardless of developmental stage, strain, or exposure to acoustic wave sorting (Fig. 7b). Fig. 7c and d displayed the representative images for offspring from a single L3 worm after 72 h of reproduction in worms exposed to SAW or control. Both groups could generate offspring normally, and the GFP signal was retained in the sorted GFP-expressing worms' offspring, as shown in Fig. S6.† Overall, these experiments show that there is not significant damage to the worms following exposure to acoustic waves, so worms sorted for genotype or GFP expression can be used in subsequent experiments.

# Conclusions

In summary, we have developed an integrated acoustofluidic worm sorting chip to sort GFP-expressing worms in a fast, accurate, and biocompatible manner. The chip is composed of an optical detection part and acoustic sorting part, in which the worm can be detected in the high-speed

Lab on a Chip **Paper** 

continuous flow by a pair of optical fibers without mechanical immobilization, and then precisely sorted by the biocompatible and contact-free surface acoustic waves. Furthermore, worms in two different development stages, L3 and L4 worms, have been sorted through our chip with different throughputs. Particularly, nearly 100% sorting purity and yield of L3 and L4 worms were achieved when the throughput was around 70 worms per min. Although the purity and yield decreased when the throughput was increased, they still remained over 90% at a throughput of around 115 worms per min, and over 80% at a throughput of around 155 worms per min, which is sufficient for most worm studies. Finally, our acoustofluidic chip is quite convenient in terms of operation and maintenance and can be integrated with other on-chip units to achieve the all-inone, versatile worm study platform.

# Conflicts of interest

T. J. H. has co-founded a start-up company, Ascent Bio-Nano Technologies Inc., to commercialize technologies involving acoustofluidics and acoustic tweezers.

# Acknowledgements

This research was supported by National Institutes of Health (R43OD024963, P42ES010356, and F32ES027306) National Science Foundation (ECCS-1807601). J. Z. thanks the China Scholarship Council (CSC).

# References

- 1 M. Cornaglia, T. Lehnert and M. A. M. Gijs, Lab Chip, 2017, 17, 3736-3759.
- 2 Y. Cho, D. A. Porto, H. Hwang, L. J. Grundy, W. R. Schafer and H. Lu, Lab Chip, 2017, 17, 2609-2618.
- 3 B. P. Gupta and P. Rezai, Micromachines, 2016, 7, 123.
- 4 M. A. Churgin, S. Jung, C. Yu, X. Chen, D. M. Raizen and C. Fang-yen, eLife, 2017, 6, e26652.
- 5 M. Stoeckius, J. Maaskola, T. Colombo, H. Rahn, M. R. Friedländer, N. Li, W. Chen, F. Piano and N. Rajewsky, Nat. Methods, 2009, 6, 745-751.
- 6 K. Chung, M. M. Crane and H. Lu, Nat. Methods, 2008, 5,
- C. B. Rohde, F. Zeng, R. Gonzalez-Rubio, M. Angel and M. F. Yanik, Proc. Natl. Acad. Sci. U. S. A., 2007, 104, 13891-13895.
- 8 E. M. Jorgensen and S. E. Mango, Nat. Rev. Genet., 2002, 3, 356-369.
- 9 Y. Yan, L. F. Ng, L. T. Ng, K. B. Choi, J. Gruber, A. A. Bettiol and N. V. Thakor, Lab Chip, 2014, 14, 4000-4006.
- 10 D. P. M. Chalfie, Y. Tu, G. Euskirchen and W. W. Ward, Science, 1994, 263, 802-805.
- 11 D. Dupuy, N. Bertin, C. A. Hidalgo, K. Venkatesan, D. Tu, D. Lee, D. Dupuy, N. Bertin, A. Carnec, A. Carvunis, J. Rosenberg, N. Svrzikapa, R. Pulak, J. Shingles, J. Reecehoyes, R. Hunt-newbury, R. Viveiros, W. A. Mohler, M. Tasan, F. P. Roth, C. Le Peuch, I. A. Hope, R. Johnsen, D. G.

- Moerman, A. Barabasi, D. Baillie and M. Vidal, Nat. Biotechnol., 2007, 25, 663-668.
- 12 S. E. Mango, Nat. Biotechnol., 2007, 25, 645-646.
- 13 M. M. Crane, K. Chung and H. Lu, *Lab Chip*, 2009, 9, 38-40.
- 14 X. Wang, R. Hu, A. Ge, L. Hu, S. Wang, X. Feng, W. Du and B. Liu, Lab Chip, 2015, 15, 2513-2521.
- 15 X. Ai, W. Zhuo, Q. Liang, P. T. Mcgrath and H. Lu, Lab Chip, 2014, 14, 1746-1752.
- 16 G. Aubry, M. Zhan and H. Lu, Lab Chip, 2015, 15, 1424-1431.
- 17 P. Rezai, S. Salam, P. R. Selvaganapathy and B. P. Gupta, Lab Chip, 2012, 12, 1831-1840.
- 18 L. Dong, M. Cornaglia, T. Lehnert and M. A. M. Gijs, Lab Chip, 2016, 16, 574-585.
- 19 G. Aubry and H. Lu, Lab Chip, 2017, 17, 4303-4311.
- 20 S. Sofela, S. Sahloul, M. Rafeie, T. Kwon, J. Han, M. E. Warkiani and Y. Song, Lab Chip, 2018, 18, 679-687.
- 21 N. Chronis, M. Zimmer and C. I. Bargmann, Nat. Methods, 2007, 4, 727-731.
- 22 J. Zhang, S. Yang, C. Chen, J. H. Hartman, P. Huang, L. Wang, Z. Tian, P. Zhang and D. Faulkenberry, Lab Chip, 2019, 19, 984-992.
- 23 D. Ahmed, A. Ozcelik, N. Bojanala, N. Nama, A. Upadhyay, Y. Chen, W. Hanna-Rose and T. J. Huang, Nat. Commun., 2016, 7, 1-11.
- 24 A. Ozcelik, J. Rufo, F. Guo, Y. Gu, P. Li, J. Lata and T. J. Huang, Nat. Methods, 2018, 15, 1021-1028.
- 25 X. Ding, Z. Peng, S.-C. S. Lin, M. Geri, S. Li, P. Li, Y. Chen, M. Dao, S. Suresh and T. J. Huang, Proc. Natl. Acad. Sci. U. S. A., 2014, 111, 12992-12997.
- 26 L. Ren, S. Yang, P. Zhang, Z. Qu, Z. Mao, P. Huang, Y. Chen, M. Wu, L. Wang, P. Li and T. J. Huang, Small, 2018, 14, 1801996.
- 27 X. Ding, P. Li, S. S. Lin, Z. S. Stratton, N. Nama, F. Guo, D. Slotcavage, X. Mao, J. Shi, F. Costanzo and T. J. Huang, Lab Chip, 2013, 13, 3626-3649.
- 28 M. Wiklund, Lab Chip, 2012, 12, 2018-2028.
- 29 A. Lenshof, C. Magnusson and T. Laurell, Lab Chip, 2012, 12, 1210-1223.
- 30 L. Y. Yeo and J. R. Friend, Annu. Rev. Fluid Mech., 2014, 46, 379-406.
- 31 D. J. Collins, A. Neild and Y. Ai, Lab Chip, 2016, 16, 471-479.
- 32 A. Marzo, S. A. Seah, B. W. Drinkwater, D. R. Sahoo, B. Long and S. Subramanian, Nat. Commun., 2015, 6, 8661.
- 33 G. Destgeer, K. H. Lee, J. H. Jung, A. Alazzam and H. J. Sung, Lab Chip, 2013, 13, 4210-4216.
- 34 D. J. Collins, B. Morahan, J. Garcia-bustos, C. Doerig, M. Plebanski and A. Neild, Nat. Commun., 2015, 6, 8686.
- 35 P.-H. Huang, C. Y. Chan, P. Li, Y. Wang, N. Nama, H. Bachman and T. J. Huang, Lab Chip, 2018, 12, 4955-4959.
- 36 W. A. Boyd, M. V. Smith and J. H. Freedman, Developmental Toxicology: Methods and Protocols, 2012, pp. 15-24.
- 37 L. Byerly, R. C. Cassada and R. L. Russell, Dev. Biol., 1976, 51, 23-33.
- 38 S. Uppaluri and C. P. Brangwynne, Proc. R. Soc. B, 2015, 282,

39 M. C. Letizia, M. Cornaglia, R. Trouillon, V. Sorrentino, L.

Lab on a Chip

- Mouchiroud, M. S. B. Sleiman, J. Auwerx and M. A. M. Gijs, Microsyst. Nanoeng., 2018, 4, 6.
- 40 C. Benedetti, C. M. Haynes, Y. Yang, H. P. Harding and D. Ron, Genetics, 2006, 174, 229-239.
- 41 Z. Mao, Y. Xie, F. Guo, L. Ren, P. Huang, Y. Chen, J. Rufo, F. Costanzo and T. J. Huang, Lab Chip, 2016, 16, 515-524.
- 42 F. Guo, Z. Mao, Y. Chen, Z. Xie, J. P. Lata, P. Li, L. Ren, J. Liu, J. Yang, M. Dao, S. Suresh and T. J. Huang, Proc. Natl. Acad. Sci. U. S. A., 2016, 113, 1522-1527.
- 43 M. Wu, K. Chen, S. Yang, Z. Wang, P. Huang, J. Mai, Z. Li and T. J. Huang, Lab Chip, 2018, 18, 3003-3010.
- 44 P. B. Muller, R. Barnkob, M. J. H. Jensen and H. Bruus, Lab Chip, 2012, 12, 4617-4627.
- 45 M. Gedge and M. Hill, Lab Chip, 2012, 12, 2998-3007.